Towards stable nickel catalysts for selective hydrogenation of biomass-based BHMF into THFDM

(article starts on next page)

Towards stable nickel catalysts for selective hydrogenation of biomass-based BHMF into THFDM

Abdenour Achour [a], Houman Ojagh [b], Phuoc Hoang Ho [a], Derek Creaser [a], Oleg Pajalic [b], Johan Holmberg [b], Louise Olsson [a,*]

[a] *Competence center for Catalysis, Chemical Engineering, Chalmers University of Technology, SE 412 96 Gothenburg, Sweden*
[b] *Perstorp AB, Industriparken, 284 80 Perstorp, Sweden*

ARTICLE INFO

ABSTRACT

Selective transformation of BHMF (2,5-bis(hydroxymethyl)furan) to THFDM (tetrahydrofuran-2,5-dimethanol) over a variety of structured Ni/S_x-Z_{1-x} catalysts was investigated. The effects of support, Ni loading, solvent, temperature, pressure, and particle size on the conversion and selectivity were studied. Among them, the 10 wt% Ni catalyst supported on the SiO_2:ZrO_2 weight ratio of 90:10 ($10NiS_{90}Z_{10}$) exhibits the best performance in terms of BHMF conversion and THFDM selectivity. Its good performance was attributed to its well-balanced properties, that depend upon the ZrO_2 content of the support in combination with SiO_2, the active Ni sites-support inter-action, and acidity/basicity ratio of each catalyst resulting in different Ni dispersions. Importantly, the $10NiS_{90}Z_{10}$ catalyst showed a stable selectivity to THFDM (>94%), with 99.4% conversion of BHMF during 2 h reaction time. Poor catalytic activity resulted from excessive ZrO_2 content (>10 wt%). The structural, textural, and acidity properties of $NiSi_{100-y}$-Zr_y catalysts, tuned by selectively varying the Ni amount from 5 to 15 wt%, were critically investigated using numerous material characterization techniques. Catalyst recycling experiments revealed that the catalyst could be recycled several times without any measurable loss of catalytic activity.

1. Introduction

The gradual depletion of petroleum resources and the global warming from conversion and utilization of fossil resources pose a threat to meet the demand for energy and chemicals, as well as to the sustainability of our society [1]. Much of the attention has been focused on renewable energy resources that are being considered as potential fossil energy alternatives. Currently, biomass is the only readily available organic carbon resource that could potentially meet the huge demand for renewable chemicals by society. As key platform chemicals, C_5-C_6 furfural and diols are of high value due to their potential use for many downstream organic syntheses. Since 5-hydroxymethylfurfural (HMF) biomass-derived compounds have a high oxygen content, their hydroxylmethyl and formyl group functionalities allow them to be converted to a variety of high added-value chemicals that can replace petroleum as a source of chemical products [2].

Among the various hydrogenation products of HMF, 2,5-bis(hydrox-ymethyl)furan (BHMF), 2,5-dimethylfuran (DMF), 5-methyl-2-furanme-thanol (MFM) [3–5], 1,6-hexanediol (HDO), 1,2,6-hexanetriol (HTO), tetrahydrofuran-2,5-dimethanol (THFDM) [6,7], and caprolactone [8,9], are particularly attractive due to their rich chemistry and potential applicability. These compounds are part of the larger families of potential industrial derivatives included in the TOP 10 most important biomass-derived platform chemicals by the U.S. Department of Energy (DOE) [10,11]. Their productions as key intermediates are of importance due to their numerous applications as building blocks in polymeric materials, as intermediates in pharmaceutical production and as biofuel additives. To obtain these desired intermediate chemicals, the reaction pathway and product distribution strongly depends on the reaction operating conditions and the type of catalyst employed.

Furans, mainly HMF and furfural (FA), can be subsequently used as precursors for the above listed products (BHMF, THFDM, and polyols), thus driving the synthesis of biobased polymers. However, efficient production of these products requires the minimization of side reactions that yield soluble and insoluble polymers [12]. Moreover, their separation from high-boiling point solvents and/or products, that may lead to thermal degradation, may be challenging. In addition to the problems of energy consumption, the impurities such as dimethyl sulfoxide

(DMSO) residuals contained in actual manufactured HMF has been reported in our previous study to have negative effects that causes a risk for catalyst deactivation [13]. Thus, the solvent of reaction plays an important role in determining the product yield or the reactivity in a chemical reaction. A recent study by Alamillo et al. showed that the selectivity to THFDM was affected by the solution-phase acidity containing HMF feed. The pretreatment with a basic ion-exchange resin resulted in an increase in pH, and thereby led to an increase of over 20% in the selectivity to THFDM using Ru catalysts [14].

The catalyst support also plays an important role in the selectivity of hydrogenation reactions. Alamillo et al. [14] studied the conversion of HMF and demonstrated that Ru supported on materials such as magnesia-zirconia, Al_2O_3, and ceria, resulted in a high yield of THFDM compared to SiO_2 [14]. Moreover, the supported catalysts containing Pt and Pd were not active for the selective hydrogenation of HMF to THFDM. They also demonstrated that Pd supported on amine functionalized Metal-Organic Frameworks (MOFs) showed preferential adsorption of the hydrogenation intermediate BHMF rather than the reactant HMF, which promotes a further hydrogeneration of BHMF to give a maximum THFDM yield of 96%. Thus, the author suggested that the minor impurities of acid mixed with HMF decreased the selectivity to THFDM [14]. It is noteworthy that Raney Ni catalysts showed high selectivity towards THFDM, with a yield of 89% over Ni-Co-Al mixed oxides and 96% yield over Ni-Pd/SiO_2; however, it is less active than metallic Ni supported catalysts for HMF hydrogenation toward THDFM [8,15].

The effect of different acid catalysts for the selective hydrogenolysis of polyols, cyclic ethers and HMF was also studied [3,16,17]. It was suggested that the acidic supports influence the product selectivity and favor the formation of ring-opening polyol products. Recent studies have revealed that THFDM can be converted to polyols including 1,6-hexanediol (HDO) and 1,2,6-hexanetriol (HTO) in very high yields [7]. This may be challenging because the hydroconversion of BHMF could result in over-hydrogenation to various byproducts, which in turn increases the difficulty for separation of byproducts [7,17]. Recent advances in the catalytic hydrogenation of HMF to produce THFDM are summarized in Table S1 (Supplementary information, SI). THFDM could be more widely used than BHMF, as it has a low probability of forming side products during polymerization [18]. A recent techno-economic evaluation of a hydrodeoxygenation process converting HMF into THFDM was conducted using Aspen Plus at our group and it was found that separation could be feasible for this system [19].

However, as far as we are aware, there are no investigations of THFDM production from conversion of BHMF reported (see Scheme 1), which is the goal in this project. In this work, we demonstrated a facile and scalable synthesis procedure for the preparation of NiS_{100-y}-Z_y catalysts (referred as Ni/SiO_2-ZrO_2). The key to this strategy is the design of a metal nickel supported catalyst that maximizes the production of the targeted compound, THFDM. This study depicts the role of the SiO_2/ZrO_2 ratio and nickel loading on catalytic performance and evaluates the stability of the composite catalyst. The effect of various solvents, temperatures, pressures, sodium hydroxide (NaOH) concentrations were also investigated to understand the properties, stability, and optimum conditions to maximize the catalytic properties and therefore enhance the activity and selectivity for THFDM formation. We found that SiO_2 and ZrO_2 can work synergistically and when the supports are optimally combined, they show excellent activity and high chemo-selectivity for the hydrogenation of BHMF into THFDM under mild reaction conditions.

2. Material and methods

2.1. Material

All of the following chemicals were of analytical grade and were used without further purification: BHMF ($\geq$ 99% purity), THFDM (98% purity), HDO (99% purity), HTO (98% purity), DMF (99% purity), MFM (99% purity), methanol (Sigma-Aldrich, Reagent Plus®, 99%), ethanol (Sigma-Aldrich, Reagent Plus®, 99%), n-butanol (Sigma-Aldrich, Reagent Plus®, 99%), n-hexanol (Sigma-Aldrich, Reagent Plus®, 99%), ZrO_2 (>98.0%, Sigma Aldrich, powder form), Amorphous SiO_2 (>99.0%, Catalyst support pellets, Alfa Aesar), nickel (II) nitrate hexahydrate ($Ni(NO_3)_2 \cdot 6 H_2O$, 98%, Sigma-Aldrich), sodium hydroxide (NaOH, 97%, Sigma-Aldrich).

2.2. Catalyst preparation

All catalysts were prepared by an incipient wetness impregnation route. Firstly, the SiO_2 and ZrO_2 supports (See Materials Section) were calcined in air at 550 °C and 750 °C respectively for 4 h. The SiO_2 pellets were crushed, ground and then sieved to a size fraction $\leq$ 250 μm. A required amount of $Ni(NO_3)_2 \cdot 6 H_2O$ was dissolved in a calculated amount of deionized water and then was added dropwise to the calcined supports or their combinations, prepared by mortar mixing. The impregned catalysts were air-dried at 110 °C for 12 h, reduced with H_2 at 450 °C for 6 h and then passivated under flowing 2% O_2 in argon at ambient temperature for 1 h. The SiO_2 and ZrO_2 mixed oxide ($S_{100-y}Z_y$) catalyst samples with y wt% of ZrO_2 and x wt% nickel will be hereafter designated as $xNiS_{100-y}Z_y$, as presented in Table 1.

2.3. Catalytic studies

The hydroconversion of BHMF was performed in a 300 mL autoclave reactor (Büchiglas, Switzerland). Typically, 5 g of BHMF was firstly dissolved into 80 g of solvent (1-butanol, ethanol, 1-propanol or 1-hexanol) in the reactor with stirring. Then, 1 g of catalysts was added into the reaction mixture. After closing the reactor, flushing with N_2 and H_2 and leak testing, the mixture was pressurized using pure hydrogen 5.5 (> 99.9995%, Aga Sweden) and heated to the desired temperature while stirring at 700 rpm. After the desired operating conditions (pressure and temperature) were reached (regarded as time zero), the product samples were collected at time zero, after 30 min and then every 1 h. The product sample was collected directly prior to cooling the reactor to room temperature.

2.4. Products analysis

Afterwards, the catalysts and liquid products were separated by vacuum filtration and then further filtered with a 0.45 μm nylon membrane filter. The catalysts were further washed by analytical grade
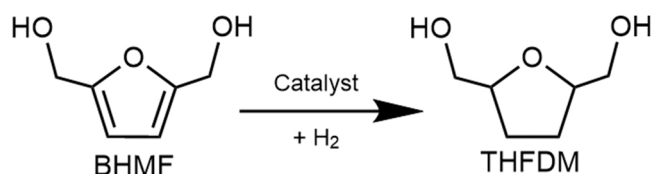
Scheme 1. The main reaction in this work.

Table 1

Catalyst sample compositions and notations.

Catalysts	Ni content, x wt%	Support, wt%		Notation $xNiS_{100-y}Z_y$
		SiO_2 (100-y)	ZrO_2 (y)	
10Ni/SiO_2	10	100	0	10NiS
10Ni/90SiO_2-10ZrO_2	10	90	10	$10NiS_{90}Z_{10}$
5Ni/90SiO_2-10ZrO_2	5	90	10	$5NiS_{90}Z_{10}$
15Ni/90SiO_2-10ZrO_2	15	90	10	$15NiS_{90}Z_{10}$
10Ni/70SiO_2-30ZrO_2	10	70	30	$10NiS_{70}Z_{30}$
10Ni/50SiO_2-50ZrO_2	10	50	50	$10NiS_{50}Z_{50}$
10Ni/10SiO_2-90ZrO_2	10	10	90	$10NiS_{10}Z_{90}$

methanol. Liquid products were collected for GC-MS analysis. The samples were injected into an Agilent GC system 7890 A coupled with an Agilent 5977 A mass spectroscopy detector equipped with a moderately polar VF1701ms column (30 m × 0.25 mm × 0.25 μm). Calibration curves of reactant and products were well correlated ($r^2 > 0.992$) within the range 250–5000 μg/mL. Relative standard deviations of retention time, and peak areas less than 5.95% were achieved. The corresponding yield, conversion, selectivity, and carbon recovery calculations are given in the supplementary information (SI).

2.5. Catalysts characterization

The details of the catalyst characterization methods have been published in our previous paper [13]. The N_2 adsorption and desorption isotherms were acquired at − 195 ℃ (TriStar 3000 gas adsorption analyzer). At first, the catalyst was dried (degassing) at 250 ℃ under vacuum for 4 h. Metal size and dispersion were determined by the CO chemisorption technique using a Micromeritics ASAP2020 Plus instrument. About 0.15 g of catalyst was first evacuated at 110 ℃ and then reduced in H_2 at 450 ℃ for 3 h. The X-ray diffractometer (Bruker D8 Advance) was used to acquire the powder XRD pattern in the 2θ range of 20–70° with a 0.016°/s scanning rate and the nickel filter. The CuKα was used as X-ray source (λ = 1.5418 Å). The Ni content of samples was determined by inductively coupled plasma and sector field mass spectroscopy (ICP-SFMS) at ALS Scandinavia AB, Luleå, Sweden. High angle annular dark field (HAADF) STEM imaging was performed on the fresh and spent catalysts using an FEI Titan 80–300, operating at 300 kV. The chemical state of the Ni phase of the catalysts was investigated with X-ray photoelectron spectroscopy (XPS) using a PHI 5000 Versa Probe III–Scanning XPS Microprobe™ system. Carbon rubber pads were situated on a sample holder. The quantity and strength of acid sites was characterized by a temperature-programmed desorption of ammonia (NH_3-TPD) technique using a manifold of gas mass flow controllers (MFC, Bronkhorst), a Differential Scanning Calorimeter (DSC, Setaram Sensys) and a mass spectrometer (MS, Hiden Analytical HPR 20). Briefly, the catalyst was pretreated at 400 °C for 2 h in Ar with flow rate of 20 mL/min. The sample was thereafter exposed to 2000 ppm NH_3 in Ar for 1 h, flushed with Ar for 1 h and thereafter the temperature ramp was conducted to 700 °C with a heating rate of 10 °C/min.

3. Results and discussion

3.1. Catalyst characterizations

The XRD patterns of the ZrO_2, SiO_2 and mixed oxides $S_{100-y}Z_y$ supports are presented in Fig. S1. The amorphous silica (SiO_2) is essentially observed as a broad characteristic peak around 22.1°. In contrast the ZrO_2 support is crystalline and matches the monoclinic mineral baddeleyite (ZrO_2). The mechanically mixed oxide $S_{100-y}Z_y$ shows a superposition of reflections of the crystalline ZrO_2 and a broad reflection of amorphous SiO_2. The presence of more than one broad amorphous band indicates that the mechanical mixing is not perfect and the Si/Zr ratios vary locally throughout the oxide, which was also confirmed by the HRTEM. Moreover, the XRD peak positions were not altered, thus there was no effect on the lattice. After the impregnation of the Ni metal (Fig. S2a), two small peaks appeared at 44.4° and 52.0°, which are attributed to the (111), and (200) planes of the cubic metallic Ni phase (JCPDS 04–0850). It also revealed reflections at 37°, 43°, and 63°, attributed to a NiO phase (JCPDS no. 471049). The intensities and positions of these reflections are somewhat different from the reference data and are associated with the formation of silicate-like structures. Of interest is the shape of the NiO peaks, which are sharp at the top but considerably broadened at the base (gray curve, Fig. S2a). This is most likely due to a bimodal size distribution of the NiO particles in the catalyst [20]. Thus, the fresh sample likely contains highly dispersed NiO species responsible for a broadening of XRD reflections, while

particles of larger sizes account for the sharp tops of these peaks.

The N_2 adsorption-desorption analysis results of ZrO_2, SiO_2 and mixed oxides $S_{100-y}Z_y$ support catalysts are listed in Table 2. It shows that the ZrO_2 support has a low BET surface area of 3.9 m^2/g and pore volume of 0.01 cm^3/g. The BET surface area of the mixed oxides $S_{100-y}Z_y$ supports, is not included for brevity, but they increased as the SiO_2 content increased from 23.6 to 90.5 m^2/g (10–90 wt%), including the pore volume 0.08—0.35 cm^3/g which was consistent with the open porosity–SiO_2 dependence (BET surface area of 101.6 m^2/g and pore volume of 0.37 cm^3/g). As shown in Table 2, the impregnation of 10 wt % of Ni on the surface of each support is decreased the specific surface area (17.7–82.5 m^2/g) and pore volume (0.06–0.26 cm^3/g) as expected. Moreover, increasing the Ni loading (5–15 wt%) resulted in a decrease in surface area. This is due to the accumulation of Ni at the mouth of pores causing less N_2 adsorption and so that the specific surface area of the catalyst decreases with an increase in wt% Ni loading. Elemental analysis by ICP-SFMS of the reduced catalysts revealed that the actual Ni loading was close to the nominal values (Table 2).

The CO chemisorption (Table 2), clearly show that the dispersion of Ni strongly depends on the support-type. The Ni dispersion gradually decreased from 22.6 to 1.2 wt% as the ZrO_2 content increased in the mixed oxides from 10 to 90 wt%. The structure of SiO_2 appears to promote better dispersion of Ni (26.2 wt%) compared to the $Si_{90}Z_{10}$ support (22.6 wt%), in line with the observed absence of Ni on the ZrO_2 support (Table 2). Moreover, the Ni dispersion is decreasing with Ni loading (Fig. S2b). From HAADF-STEM (Fig. S3), it is found that the ZrO_2 particles are randomly distributed and isolated from SiO_2. This observation is confirmed by XRD patterns that indicated non-perfect mixing. STEM-EDS images of the reduced Ni-metallic catalysts show the presence of well-defined nickel particles, deposited mostly on the SiO_2 support (Fig. S3). The HAADF-STEM images of the reduced-passivated Ni-metallic catalysts show that metallic Ni particles were well dispersed on SiO_2 (Fig. S4). These particles have sizes of 5–10 nm, which is in good agreement with the Ni particle sizes obtained by the CO-TPD measurements (Table 2).

The total amount of acidic sites on the catalysts were calculated (Table 2) from the NH_3-TPD spectra (Fig. S5). All the $Ni/S_{100-y}Z_y$ catalysts except ZrO_2 exhibit a NH_3-TPD spectrum with two NH_3 desorption peaks at 220 ℃ (corresponding to weak acid sites) and around 500 ℃ (corresponding to strong acid sites). As shown in Fig. S5, some difference in the acidic properties, both the acid strength and amount of the acidic sites, was observed after the introduction of ZrO_2. It has been reported that the addition of ZrO_2 in SiO_2 can decrease the density of acidic sites [14,21]. These findings are corroborated by the results presented herein showing that the density of acid sites decreased when increasing the ZrO_2 content (see Fig. S5). The decrease is close to linear with an R2 of 0.95. Charisiou et al. [21] also reported that the surface basicity of

Table 2
Bulk and surface properties of SiO_2 support, ZrO_2 support, Catalysts.

Samples	ICP-MS	N_2 Adsorption-Desorption		CO chemisorption		NH3 uptake*
		S_{BET} (m^3/g)	Pore Volume (cm^3/g)	Ni Dispersion[a] (wt%)	Ni Particle[b] size (nm)	
10NiS$_{100}$	-	90.9	0.28	26.2	3.9	67.9
5NiS$_{90}$Z$_{10}$	5.5	84.5	0.25	34.3	2.9	64.4
10NiS$_{90}$Z$_{10}$	10.7	82.5	0.24	22.6	4.5	64.4
15NiS$_{90}$Z$_{10}$	16.1	71.8	0.26	16.8	6.0	64.4
10NiS$_{70}$Z$_{30}$	-	68.0	0.23	14.9	6.8	46.4
10NiS$_{50}$Z$_{50}$	-	59.6	0.18	15.4	6.6	50.7
10NiS$_{10}$Z$_{90}$	-	17.7	0.06	1.2	84.2	13.9
ZrO$_2$*	-	3.9	0.01	-	-	7.1

* BET and NH_3-TPD measured on supports
[a] Direct reduction in H_2 at 450 ℃ for 3 h
[b] Hemisphere shape

SiO$_2$-ZrO$_2$ is lower than that of ZrO$_2$ and they found the surface of SiO$_2$-ZrO$_2$ consists of a low number of Zr^{4+}–O^{2-} acid-base centers and a large amount of acidic Zr^{4+} centers. Moreover, the above analysis shows that the addition of ZrO$_2$ to SiO$_2$ decreases the specific surface area, and the pore volume (see Table 2). This is expected since the SiO$_2$ support had a BET surface area of 101.8 m^2/g and the ZrO$_2$ only 3.9 m^2/g. Thus, adding ZrO$_2$ content influences the physicochemical properties of Ni/S$_{100-y}$Z$_y$ catalysts and their catalytic performance. The acid/base ratio increases in the order of SiO$_2$ > S$_{100-y}$Z$_y$ > ZrO$_2$. Table 2 also gives the amount of NH$_3$ adsorbed on the various catalysts. The acidity of the S$_{90}$Z$_{10}$ support (64.4 mmol NH$_3$/g cat) was the highest in the series of mixed oxides.

XPS analysis was undertaken to estimate the oxidation states of the Ni as well as to understand the metal–support interactions in the NiS$_{100-y}$Z$_y$ catalysts. The Ni 2p XPS images of the 10NiS$_{90}$Z$_{10}$ catalyst are shown in Fig. S6. Two major peaks were noted at 855.2 and 872.6 eV, corresponding to Ni 2p$_{3/2}$ and Ni 2p$_{1/2}$ in an area ratio of 2:1. These peaks are attributed to Ni in the form of oxide and hydroxide phases. Additionally, a peak located at 852.1 eV in the figure indicates that the metallic nickel (Ni^0) phase is present on the reduced-passivated catalyst surface.

3.2. Effect of various supports

The nature of support used in this study led to the effective hydrogenation which has been reported in our earlier study [13]. Based on the literature, a degree of typical acid/base properties favors certain selective reactions. For example, deoxygenation is favored by an acidic nature and hydrogenation by a bifunctional supported catalyst with an active metal [16]. Thus, the physical-chemical character of the support is essential to influence the kinetics of the reactions and can involve an enhancement of the overall hydrogenation process. The effect of the
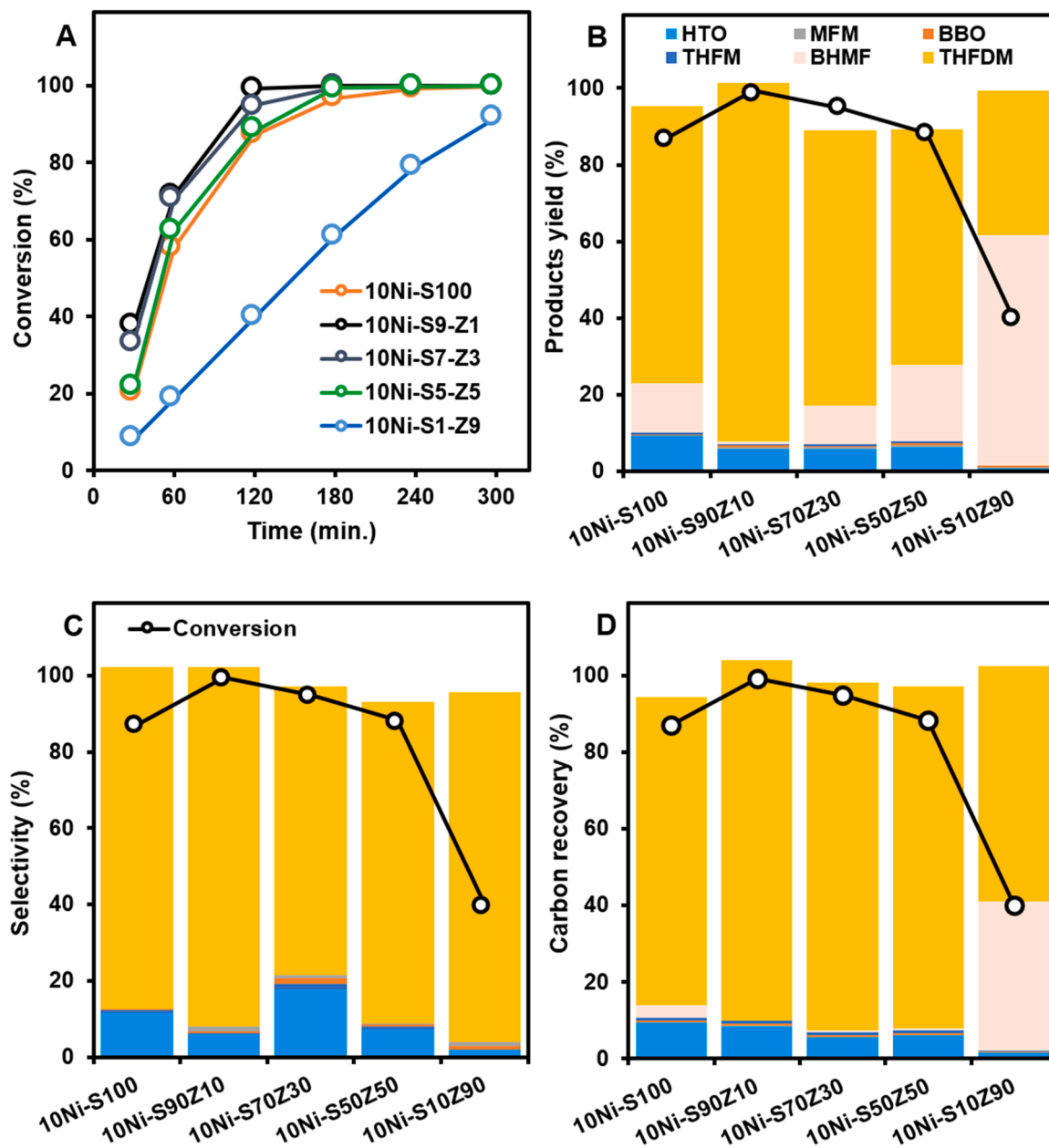

Fig. 1. Effect of supports on BHMF conversion over 300 min reaction time (a) and product yield (b), product selectivities (c) and carbon recovery indicating product contributions (d) after 120 min reaction time over various 10Ni- S$_{100-y}$Z$_y$ catalysts. The reactions were performed at 180 °C, 75 bar H$_2$, 5 g of BHFM, 80 g of butanol as a solvent, and catalyst loading of 1 g.

$S_{100-y}Z_y$ support for hydrogenation of BHMF was investigated by incorporating Nickel (Ni) as an active site over various acid-base supports, as shown in Table 1 and Fig. 1.

The relative acid/base strength tuned the selectivity and conversion of BHMF (Fig. 1). The conversion of BHMF was observed for all $10NiS_{100-y}Z_y$ catalysts as a function of time. Without the presence of ZrO_2 support, $10NiS_{100}$ showed only 87% BHMF conversion, yielding 72.1% THDFM within the reaction time of 2 h. The lowest conversion found was for high ratio ZrO_2 support, $10NiS_{10}Z_{90}$, with BHMF conversion of 39.9% at 180 ºC under 75 bar H_2 pressure after 2 h of reaction time, with the lowest yield of 37.7% for THFDM (Fig. 1b). The selectivity to THFDM was also affected by adding ZrO_2 to SiO_2 (Fig. 1c). These observations reveal that an appropriate $S_{100-y}Z_y$ composite is most favorable when using a lower amount of ZrO_2, which slightly changed the acidity of $S_{90}Z_{10}$ compared to SiO_2, leading to a THFDM selectivity of 94.7%. Despite the high surface area and Ni dispersion of SiO_2, as shown

in Table 2, THFDM was formed with lower selectivity (72.1%) compared to the most active catalyst ($S_{90}Z_{10}$), which may due to an insufficient adjustment of the acid-base balance of the support. It has also been suggested that the addition of silica over Ru-black decreases the selectivity to THFDM and increased the formation of polyols, indicating the effect of the acidity of silica [14]. Thus, the presence of the $S_{100-y}Z_y$ mixed oxide has a clear effect on the product distribution and strongly affects the selectivity towards the THFDM formation as demonstrated in Fig. 1. Although a better Ni dispersion was achieved over the $10NiS_{100}$, $10NiS_{90}Z_{10}$ favors total conversion of BHMF and higher THFDM selectivity. Note that gas formation was likely minor as the total carbon recovery reached 94.5–101.2% (Fig. 1d). To conclude, the $10NiS_{90}Z_{10}$ showed an excellent catalyst performance with the achievement of 99.3% BHMF conversion as well as 94.7% THDFM selectivity in the 2 h reaction time at 180 ºC.
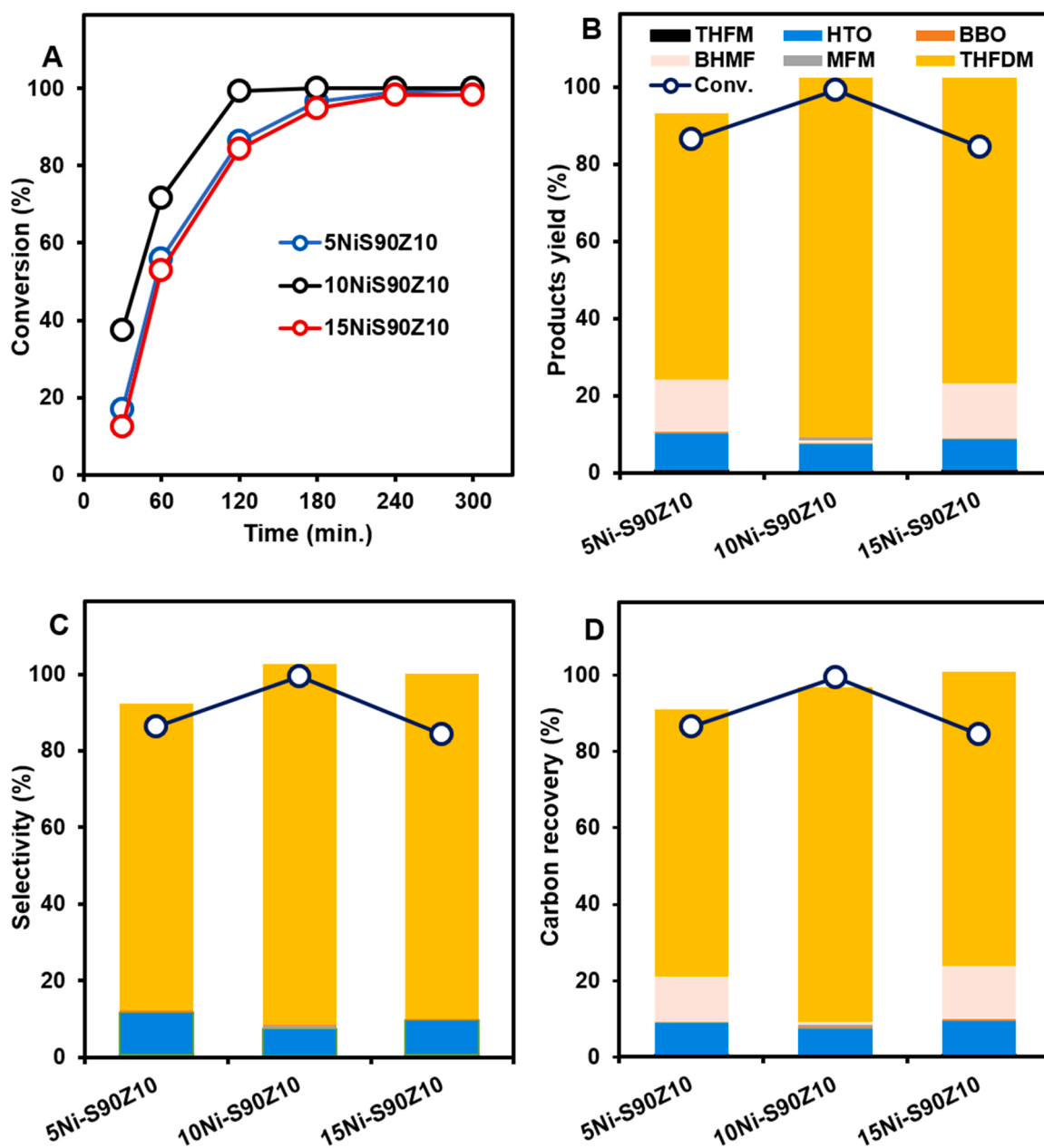

Fig. 2. Effect of Ni loadings on BHMF conversion (a) product yields (b), products selectivities (c) and carbon recovery indicating product contributions (d) after 120 min reaction time over various Ni-$S_{90}Z_{10}$ catalysts. The reactions were performed at 180 ºC, 75 bar H_2, 5 g of BHFM, 80 g of butanol as a solvent, and catalyst loading of 1 g.

3.3. Catalyst Ni loading

The effects of Ni content on the $S_{90}Z_{10}$ support were also investigated to probe the selectivity for BHMF hydrogenation. The conversion, product yields, selectivities, and product carbon recovery are given in Fig. 2. The increase in the content of Ni from 5 to 10 wt% enhanced the catalytic activity due to the existence of more active sites in the high Ni loading catalyst. The conversion of BHMF increased from 86.5% to 99.3% after 2 h reaction time (Fig. 2a). In contrast, an additional increase in Ni content to 15 wt% declined the BHMF conversion to 90%. When increasing the Ni loading the dispersion decreased, as shown in Table 2. However, the total amount of available Ni sites is still about 11% higher for the 15 wt% Ni sample compared to 10 wt% sample. These results suggests that the reaction also likely is structure sensitive and not only dependent on the number of exposed sites. Moreover, it was observed that the largest amount of byproduct during BHMF hydrogenation was HTO. The HTO remained stable after 2 h reaction time with the selectivity of 9.7%, 7.1% and 10.2% for the three Ni loadings, respectively. This results in that the THFDM yield for the 10 wt% Ni was slightly higher than the other samples. In addition, the 10 wt% Ni showed a faster reaction than 5 and 15 wt% Ni for BHMF hydrogenation (Fig. 2). Accordingly, the overall selectivity for THFDM is dependent on both the number of catalytically active sites that increase relative rate of hydrogenation as well as the structure of the nickel particles. In addition, the acid-base balance of the support used is also important as seen from the results in Fig. 1. Note that the gas product formation was minor since the total carbon recovery ranged from 93.3% to 100.5% (Fig. 2d).

3.4. Solvent comparison

The hydrogenation of BHMF was further carried out in a variety of solvents using 1-butanol, ethanol, 1-propanol and 1-hexanol to understand primarily their influences on BHMF conversion and selectivity. Apart from dissolving the solid BHMF into a liquid form, the solvents can also improve the heat and mass transfer rates and enhance the miscibility of the reaction mixture. Moreover, low molecular weight alcohols such as ethanol, propanol and ethylene glycol are among the preferred choices as hydrogen donor solvents, however at higher temperature and pressure (e.g., 300–500 °C, 30–100 bar H_2) [22,23]. For instance, ethanol has been reported to act as a hydrogen donor molecule as reported for the hydrotreatment of guaiacol at 300 °C and 50 bar of hydrogen pressure [23]. In this solvent comparison study, the maximum

temperature was 180°C, which suggests that the hydrogen donated from solvents (ca. 80 g) is probably minor, considering it should require higher temperature to produce H_2 from the solvents. Under lower hydrogen pressure at 180°C (20 bar, Table 4), BHMF conversion and THFDM yields were considerably lower after 1 h reaction time, corresponding to 12%, and 15%, respectively. This observed strong influence of hydrogen pressure on conversion indicates that the pure hydrogen supplied was mainly affecting the reaction rather than hydrogen donated from alcohols.

As shown in Fig. 3 the solvents were found to play a crucial role in the conversion and selectivity. Butanol showed the highest BHMF conversion of 99.7% with an increase and then stable THFDM selectivity as a function of time, suggested that butanol was a favorable solvent for the selective hydrogenation of BHMF into THFDM. Taking the solvent-solute interaction into consideration, after 2 h of reaction time, the observed hydroconversion and THFDM selectivity varied with solvent in the following order: 1-butanol > ethanol > 1-propanol > 1-hexanol. This implies that 1-butanol proved to be a highly efficient solvent and chemically stable. It is noteworthy to mention that none of the used solvents, except 1-hexanol, reacted during the reaction. 1-hexanol formed other aliphatic alcohols and hydrocarbons such as i.e., 1-Octanol, 3-octanol, and hexane (Fig. S7, chromatogram).

3.5. Effects of reaction temperature on BHMF hydrogenation

The effects of hydrogenation temperature on reaction conversion as indicated by changes in the selectivity of THFDM are illustrated in Table 3. This set of hydrogenation experiments were conducted in the temperature range 60 – 180 °C while maintaining all other parameters constant (pressure of 75 bar H_2 with $10NiS_{90}Z_{10}$ catalyst and 1-butanol as a solvent). As expected, the BHMF conversion and THFDM yield increased from 10.2% to 99.4% and 10.1–94.6% respectively with increasing the reaction temperature from 60 to 180 °C at 120 min reaction time. It was also revealed that the reaction was feasible even at a low temperature of 60 °C, although the conversion was only 10.2% with the major product formed being THDFM (98.3%). On further increasing the temperature to 130 °C, the BHMF conversion achieved was 42.5% with selectivity to THFDM still maintained as high as 93%. Moreover, another product formed was HTO with 3.1% yield (not shown for brevity). A further rise in temperature to 180 °C led to an increase in HTO yield (7%). A regression analysis of the rates of formation of THFDM and HTO indicated that their apparent activation energies were
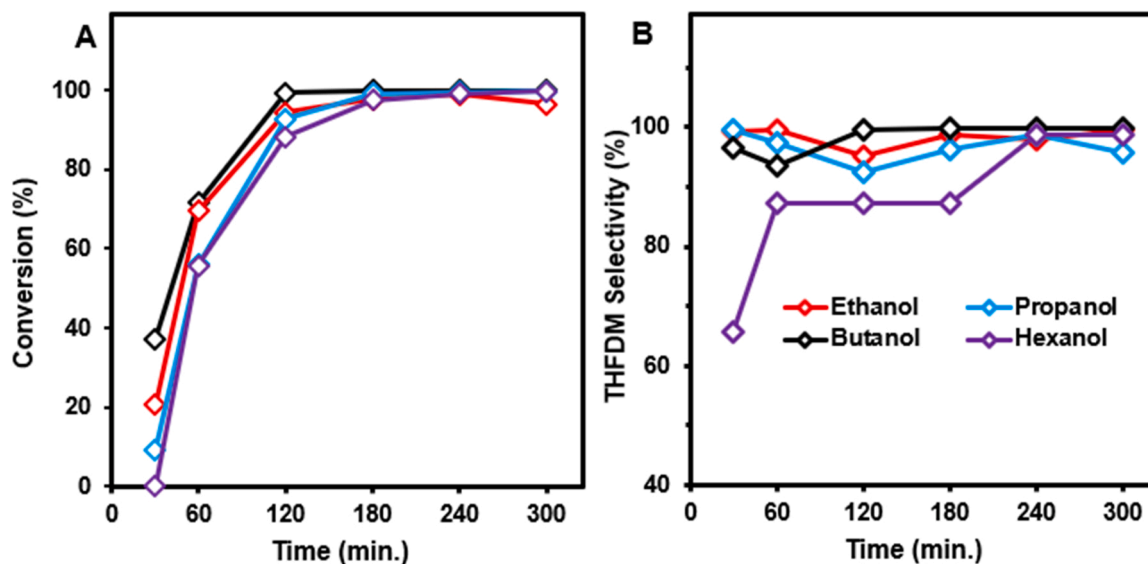

Fig. 3. Effect of the solvent on BHMF hydrogenation (a) conversion (b) selectivity for THFDM and HTO over the course of 300 min reaction time. The reactions were performed at 180 °C, 75 bar H_2, 5 g of BHFM, 80 g of solvent, and catalyst loading of 1 g 10Ni-$S_{90}Z_{10}$.

Table 3
Effects of reaction temperatures on product distribution for BHMF hydrogenation at various reaction times. All reaction were run with 5 g BHMF and 1 g $10NiS_{90}Z_{10}$ catalyst in butanol at 75 H_2 bar.

Temperature (°C)	Reaction time (min)	BHMF Conversion (%)	Selectivity (%)				
			THFM	BBO	MFM	THFDM	HTO
60	60	2.5	0.7	0.0	0.7	80.7	0.0
	120	10.2	0.2	0.0	0.2	98.3	0.0
90	60	8.5	0.0	0.0	0.2	91.7	0.0
	120	22.3	0.0	0.0	0.2	99.7	0.0
130	60	12.6	0.0	0.0	0.3	95.9	1.6
	120	42.5	0.0	0.0	0.2	93.2	7.4
150	60	28.2	0.0	0.0	0.4	94.0	2.6
	120	50.3	0.0	0.0	0.5	89.5	7.6
180	60	71.8	0.2	0.5	0.8	92.7	6.5
	120	99.4	0.4	0.4	0.5	95.1	7.0

30.4 and 31.1 kJ mol^{-1} respectively (see ESI for details, Fig. S8). Considering the small differences in these values relative to the expected uncertainties in evaluation, it can be concluded that the overall selectivity for HTO did not significantly increase with temperature and thus a high selectivity for THFDM was maintained. This finding indicates there is little difference in the energies required for hydrogenation of the C═C double bonds of the furfural ring versus hydrolysis to open the furfural ring. At the highest temperature of 180 ℃, the conversion of BHMF reached 99.4%, and THFDM selectivity steadily increased to 95.1% whereas the other major product was HTO at maximal 7% selectivity for reaction time of 120 min

3.6. Effect of hydrogen pressure

The effect of the reaction pressure over the $10NiS_{90}Z_{10}$ catalyst was also studied and the results are shown in Table 4. Both BHMF conversion and THFDM yield increased with the reaction pressure. The conversion of BHMF was less than 30% with H_2 pressure of 20 bar, where THFDM was produced with 29% yield and 98.3% selectivity. A further increase in the H_2 pressure to 75 bar led to increased THDFM yields with a maximum yield of 94.6% (Table 4). As a function of the H_2 pressure, the yield of HTO was enhanced as well. In addition, traces of BBO, MFM and THFM were also identified and quantified with levels of selectivity less than 1%. A regression analysis of the rates of formation of THFDM and HTO between the time points in Table 4, indicated that the apparent orders of the rates of formation with respect to H_2 were 1.6 and 0.5 respectively (see details in Fig. S9). Since formation of THFDM has a stronger dependence on H_2 pressure (higher order dependence on. H_2), it can be concluded that higher pressure favors selective hydrogenation of BHMF to THFDM. Therefore, to achieve a high conversion and selectivity for THFDM, a pressure of 75 bar was chosen throughout the investigations for optimization of the other parameters.

3.7. Effect of pH

We also examined the effect of pH by introducing NaOH over the

$10NiS_{90}Z_{10}$ catalyst. The $10NiS_{90}Z_{10}$ catalyst was initially pretreated with the addition of NaOH as a base at different pH values of 8, 11 and 14. The pretreated catalysts were investigated under the optimum reaction conditions. After the reaction for 5 h, the catalyst was filtered out from the reaction products and the nickel content of the solid catalysts were analyzed via ICP-MS. The results shown in Fig. 4 suggest that poor catalytic performance was observed under alkaline conditions compared to the untreated catalyst (Fig. 4a, black line). Fig. 4b shows the correlation between the Ni content of the spent catalysts and the pH of the reaction solutions. It also indicates that a significant leaching occurred from the $10NiS_{90}Z_{10}$ catalyst, particularly at pH 14, corresponding to the lowest Ni content (< 10 wt%, see Fig. 5B). However, higher BHFM conversion was observed, and surprisingly with higher selectivity of THFDM for pH 14 compared to the pH values 8 and 11 (Fig. 4a). This behavior is consistent with findings in literature that pretreatment of the catalyst with a basic ion-exchange resin resulted in an increase in pH, and thereby led to an increase of over 20% in the selectivity to THFDM using Ru catalysts [14].

To gain information on the degree of nickel leaching, a comparison of the spent catalysts was conducted via ICP-MS, XPS and HRTEM. The HAADF-STEM imaging (Fig. S12) of the spent catalyst after the addition of a reductive agent provided direct evidence for the formation of metallic Ni nanoparticles, particularly above pH 11. This indicates that the pH at higher solution-phase basicity influences the formation of metallic Ni nanoparticles (HAADF-STEM, Fig. S12) by dissolving Ni species which might actively enhance the BHMF conversion and THFDM selectivity via leaching and thereafter redeposition of Ni nanoparticle onto the support with higher dispersion. As it can be also observed in Fig. S13, the relative strength of Ni2p intensity reduced remarkably as a function of the pH strength, which indicates the smaller particle size.

3.8. Catalyst recycling

A multiple cycle experiment for BHMF hydroconversion using the $10NiS_{90}Z_{10}$ catalyst in butanol at 180 ℃, 75 bar for 5 h was performed to investigate the long-term stability of the $10NiS_{90}Z_{10}$ catalyst, as shown

Table 4
Effects of reaction pressure on product distribution for BHMF hydrogenation at various reaction times. All reaction were run with 5 g BHMF and 1 g $10NiS_{90}Z_{10}$ catalyst in butanol at 180 ℃.

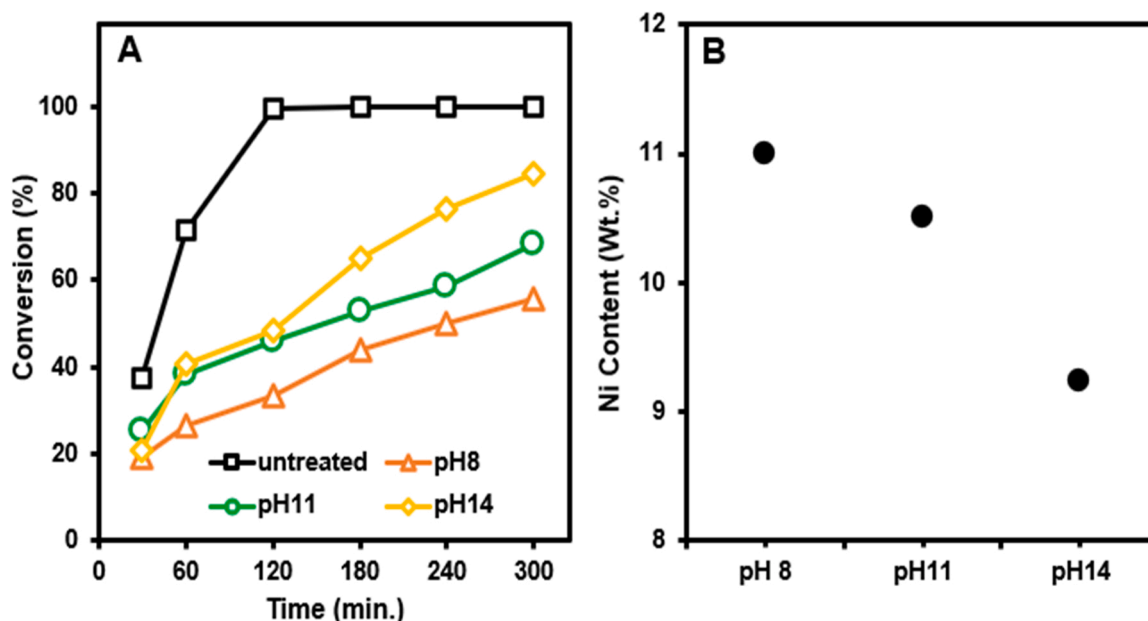| Pressure (bar)	Reaction time (min)	BHMF Conversion (%)	Selectivity (%)				
			THFM	BBO	MFM	THFDM	HTO
20.0	60	12.0	0.0	3.2	2.2	97.4	2.0
	120	29.5	0.1	1.3	1.9	98.3	2.0
40.0	60	31.1	0.2	1.3	1.9	95.5	6.2
	120	73.0	0.2	0.6	0.9	97.0	5.7
60.0	60	50.4	1.0	0.9	1.3	94.7	7.5
	120	87.4	0.8	0.6	0.6	95.5	7.9
75.0	60	79.3	0.2	0.4	0.6	96.6	7.8
	120	99.7	0.3	0.3	0.6	96.8	6.6

Fig. 4. Influence of NaOH addition on BHMF hydrogenation over 10NiS$_{90}$Z$_{10}$ catalyst. (a) Influence of treatment of catalyst with NaOH on BHMF conversion (b) Ni content of the spent catalyst measured by ICP-MS. Reaction conditions: 180 °C, 75 bar H$_2$ pressure, 300 min reaction time, 5 g BHMF in 80 g Butanol, 1 g of 10NiS$_{90}$Z$_{10}$ catalyst.
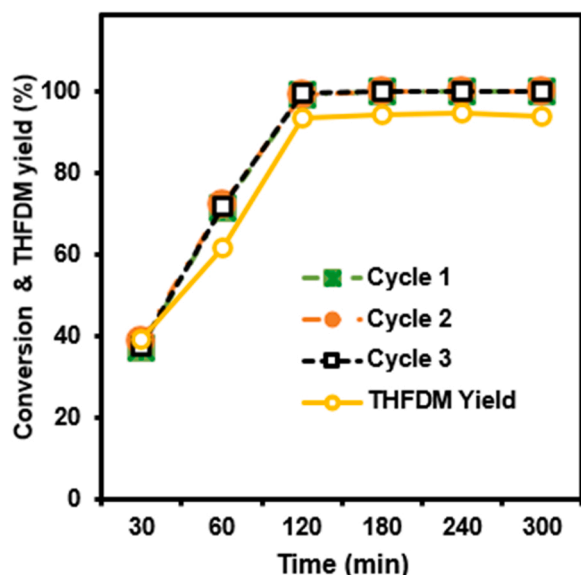

Fig. 5. Repeatability of catalyst 10NiS$_{90}$Z$_{10}$ for BHMF catalytic hydrogenation conversion up to three runs and average THFDM yield of three cycles. The reactions were performed at 180 ℃, 75 bar H$_2$, 5 g of BHFM, 80 g of butanol as a solvent, and catalyst loading of 1 g.

in Fig. 5. For this purpose, the spent catalyst following each cycle was recovered and washed with ethanol to remove the adsorbed products, dried at 80 ℃ and then regenerated by reduction at 450 ℃ at 15 bar of H$_2$. Then the catalyst was used for the next cycle under identical reaction conditions. It can be seen that over the three cycles, with varying reaction times, the conversion of BHMF and the selectivity for THFDM showed an excellent reproducibility, indicating that the catalyst could be reused without a significant decrease in activity. Although the conversion and yield were lower at shorter reaction times of 30 and 60 min, the stability over the cycles was maintained. The morphology and chemical composition of the 10NiS$_{90}$Z$_{10}$ catalyst after the stability test was investigated via XRD, XPS, and TEM. The XRD patterns of catalysts

before and after recycling were identical as shown in Fig. S10a, indicating no obvious change in the phase crystallinities was observed. Besides, the XPS results revealed that the Ni element is well-preserved, confirming the chemical stability of the catalyst (Fig. S10b). It is found that the relative strength of the metallic nickel (Ni^0, 852.1 eV) phase in the catalyst increased after the multi-cycle reaction test, implying that reduction of the catalyst surface occurred during the long-term hydroconversion reaction. The HAADF-STEM images of Fig. S11 provided direct evidence that Ni particles were well maintained after the recycle test, which can be strong evidence supporting the stability of 10NiS$_{90}$Z$_{10}$ catalyst.

3.9. Reaction pathways

The reductive transformation of BHMF also offers interesting opportunities for the preparation of polymer intermediates which more likely depends on the catalysts used [18]. THFDM is the dominant reaction product over the Ni-S$_{90}$Z$_{10}$ catalyst (Scheme 2a). THFDM, in turn, can undergo ring opening leading to the formation of HTO (Scheme 2b), which has been observed from 130 ℃ (Table 3) and might increase under more severe conditions. However, the Ni-S$_{10}$Z$_{90}$ catalyst (Fig. 1) is not particularly active for ring opening hydrogenation in contrast to the 10Ni-S$_{90}$Z$_{10}$ catalyst studied in this work. However, the Ni-S$_{10}$Z$_{90}$ catalyst was not so active towards THFDM with the lowest selectivity of 37.7% and conversion of 39.9% at 180 ℃ under 75 bar pressure after 2 h of reaction time. Depending on the employed catalyst, hydrogenolysis of the hydroxymethyl groups of BHMF and THFDM can simultaneously occur, leading to the formation of MFM and THFM (Schemes 2c and 2d). These side-reactions had however minor yields (less than 1%) at 180 ℃ under 75 bar pressure after 2 h of reaction time.

4. Conclusions

In summary, the catalytic hydrogenation of BHMF to THFDM has been probed for the first time over a reduced metal NiS$_{100-y}$Z$_y$ catalyst. At the best reaction conditions, i.e., 180 °C, 75 bar H$_2$ and reaction time of 2 h, the 10NiS$_{90}$Z$_{10}$ catalyst exhibited high catalytic activity with BHMF conversion of 99.4% with a yield of 94.6% for THFDM. The influence of coexistence of ZrO$_2$ and SiO$_2$, although as an imperfectly
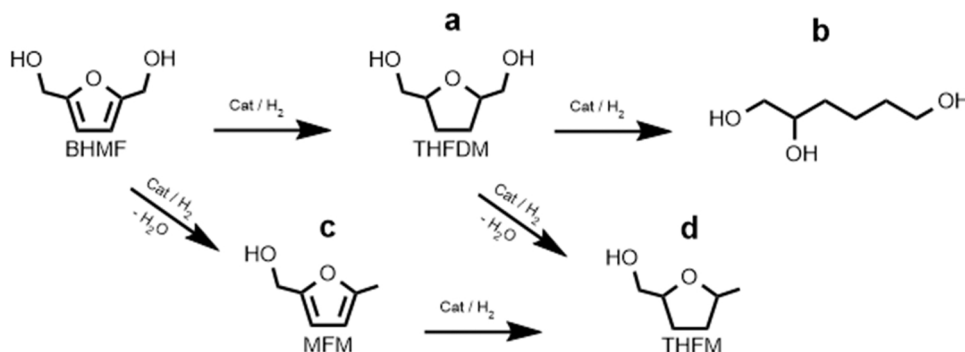
Scheme 2. Proposed pathways for furanic ring hydrogenation (a and b), and deoxygenation (c and d).

mixed composite, was essential to give a high catalytic performance. The limited addition of ZrO_2 afforded a partial reduction in alkalinity of the support SiO_2 and resulted to be beneficial for enhancing the conversion of BHMF and THFDM selectivity. In addition, the Ni dispersion of the mixed support catalyst has been found to be essential for an efficient THFDM production. The studies conducted at various solvents indicated that the reaction pathway for THFDM synthesis from BHMF is preferably proceeded using butanol as a solvent. It was also found that the reaction temperature has low effect on selectivity whereas higher H_2 pressure favored the selective formation of THFMD. Based on the high activity, recyclability, and controllability, the $10NiS_{90}Z_{10}$ catalyst for conversion of BHMF to THFDM has the potential to produce THFDM from a biomass-based precursor of BHMF, which fits well as a green conversion process.

CRediT authorship contribution statement

Abdenour Achour: Conceptualization, Investigation, Formal analysis, Writing – original draft. **Houman Ojagh:** Conceptualization, Investigation, Formal analysis, Writing – review & editing. **Phuoc Hoang Ho:** Formal analysis, Writing – review & editing. **Derek Creaser:** Conceptualization, Supervision, Writing – review & editing. **Oleg Pajalic:** Conceptualization, Supervision, Writing – review & editing, Funding acquisition. **Johan Holmberg:** Conceptualization, Supervision, Writing – review & editing, Funding acquisition. **Louise Olsson:** Conceptualization, Supervision, Writing – review & editing, Funding acquisition.

Declaration of Competing Interest

The authors declare that they have no known competing financial interests or personal relationships that could have appeared to influence the work reported in this paper.

Data Availability

Data will be made available on request.

Acknowledgements

distillation equipment.

Appendix A. Supporting information

Supplementary data associated with this article can be found in the online version at doi:10.1016/j.jece.2023.109461.

References

[1] J.-F. Mercure, P. Salas, P. Vercoulen, G. Semieniuk, A. Lam, H. Pollitt, P.B. Holden, N. Vakilifard, U. Chewpreecha, N.R. Edwards, J.E. Vinuales, Reframing incentives for climate policy action, Nat. Energy 6 (2021) 1133–1143, https://doi.org/10.1038/s41560-021-00934-2.

[2] X. Tang, J. Wei, N. Ding, Y. Sun, X. Zeng, L. Hu, S. Liu, T. Lei, L. Lin, Chemoselective hydrogenation of biomass derived 5-hydroxymethylfurfural to diols: Key intermediates for sustainable chemicals, materials and fuels, Renew. Sustain. Energy Rev. 77 (2017) 287–296, https://doi.org/10.1016/j.rser.2017.04.013.

[3] X. Tong, Y. Ma, Y. Li, Biomass into chemicals: conversion of sugars to furan derivatives by catalytic processes, Appl. Catal. A Gen. 385 (2010) 1–13, https://doi.org/10.1016/j.apcata.2010.06.049.

[4] M. Djokic, H.H. Carstensen, K.M. Van Geem, G.B. Marin, The thermal decomposition of 2,5-dimethylfuran, Proc. Combust. Inst. 34 (2013) 251–258, https://doi.org/10.1016/j.proci.2012.05.066.

[5] J. Jae, W. Zheng, A.M. Karim, W. Guo, R.F. Lobo, D.G. Vlachos, The role of Ru and RuO2 in the catalytic transfer hydrogenation of 5-hydroxymethylfurfural for the production of 2,5-dimethylfuran, ChemCatChem 6 (2014) 848–856, https://doi.org/10.1002/cctc.201300945.

[6] J. Tuteja, H. Choudhary, S. Nishimura, K. Ebitani, Direct synthesis of 1,6-hexanediol from HMF over a heterogeneous Pd/ZrP catalyst using formic acid as hydrogen source, ChemSusChem 7 (2014) 96–100, https://doi.org/10.1002/cssc.201300832.

[7] J. He, S.P. Burt, M. Ball, D. Zhao, I. Hermans, J.A. Dumesic, G.W. Huber, Synthesis of 1,6-hexanediol from cellulose derived tetrahydrofuran-dimethanol with Pt-WOx/TiO2 catalysts, ACS Catal. 8 (2018) 1427–1439, https://doi.org/10.1021/acscatal.7b03593.

[8] T. Buntara, S. Noel, P.H. Phua, I. Melián-Cabrera, J.G. De Vries, H.J. Heeres, Caprolactam from renewable resources: Catalytic conversion of 5-hydroxymethylfurfural into caprolactone, Angew. Chem. - Int. Ed. 50 (2011) 7083–7087, https://doi.org/10.1002/anie.201102156.

[9] Y. Nakagawa, K. Tomishige, Total hydrogenation of furan derivatives over silica-supported Ni-Pd alloy catalyst, Catal. Commun. 12 (2010) 154–156, https://doi.org/10.1016/j.catcom.2010.09.003.

[10] T. Werpy, G. Petersen, Rep.: Top. Value Added Chem. Biomass-.-. (2004), https://doi.org/10.2172/926125.

[11] J.J. Bozell, G.R. Petersen, Technology development for the production of biobased products from biorefinery carbohydrates—the US Department of Energy's "top 10" revisited, Green. Chem. 12 (2010) 539–555, https://doi.org/10.1039/b922014c.

[12] B.S. Solanki, C.V. Rode, Selective hydrogenolysis of 5-(hydroxymethyl)furural over Pd/C catalyst to 2,5-dimethylfuran, J. Saudi Chem. Soc. 23 (2019) 439–451, https://doi.org/10.1016/j.jscs.2018.08.009.

[13] H. Ojagh, A. Achour, P.H. Ho, D. Bernin, D. Creaser, O. Pajalic, J. Holmberg, L. Olsson, Effect of DMSO on the catalytical production of 2{,}5-bis(hydoxymethyl) furan from 5-hydroxymethylfurfural over Ni/SiO2 catalysts, React. Chem. Eng. 7 (2022) 192–200, https://doi.org/10.1039/D1RE00255D.

[14] R. Alamillo, M. Tucker, M. Chia, Y. Pagán-Torres, J. Dumesic, The selective hydrogenation of biomass-derived 5-hydroxymethylfurfural using heterogeneous

catalysts, Green. Chem. 14 (2012) 1413–1419, https://doi.org/10.1039/C2GC35039D.

[15] N. Perret, A. Grigoropoulos, M. Zanella, T.D. Manning, J.B. Claridge, M. J. Rosseinsky, Catalytic response and stability of nickel/alumina for the hydrogenation of 5-hydroxymethylfurfural in water, ChemSusChem 9 (2016) 521–531, https://doi.org/10.1002/cssc.201501225.

[16] M. Chia, Y.J. Pagán-Torres, D. Hibbitts, Q. Tan, H.N. Pham, A.K. Datye, M. Neurock, R.J. Davis, J.A. Dumesic, Selective hydrogenolysis of polyols and cyclic ethers over bifunctional surface sites on rhodium–rhenium catalysts, J. Am. Chem. Soc. 133 (2011) 12675–12689, https://doi.org/10.1021/ja2038358.

[17] H. Cai, C. Li, A. Wang, T. Zhang, Biomass into chemicals: One-pot production of furan-based diols from carbohydrates via tandem reactions, Catal. Today 234 (2014) 59–65, https://doi.org/10.1016/j.cattod.2014.02.029.

[18] B.M. Stadler, C. Wulf, T. Werner, S. Tin, J.G. de Vries, Catalytic approaches to monomers for polymers based on renewables, ACS Catal. 9 (2019) 8012–8067, https://doi.org/10.1021/acscatal.9b01665.

[19] M. Niemeyer, I. Lyngso, A Techno-Economic Evaluation of a HDO Process Converting HMF into THFDM, Master's thesis in Innovative and Sustainable Chemical Engineering, Chalmers University of Technology, 2022.

[20] W. Yin, R.H. Venderbosch, S. He, M.V. Bykova, S.A. Khromova, V.A. Yakovlev, H. J. Heeres, Mono-, bi-, and tri-metallic Ni-based catalysts for the catalytic hydrotreatment of pyrolysis liquids, Biomass-.-. Convers. Biorefinery 7 (2017) 361–376, https://doi.org/10.1007/s13399-017-0267-5.

[21] N.D. Charisiou, K.N. Papageridis, G. Siakavelas, V. Sebastian, S.J. Hinder, M. A. Baker, K. Polychronopoulou, M.A. Goula, The influence of SiO2 doping on the Ni/ZrO2 supported catalyst for hydrogen production through the glycerol steam reforming reaction, Catal. Today 319 (2019) 206–219, https://doi.org/10.1016/j.cattod.2018.04.052.

[22] C. Li, X. Zhao, A. Wang, G.W. Huber, T. Zhang, Catalytic transformation of lignin for the production of chemicals and fuels, Chem. Rev. 115 (2015) 11559–11624, https://doi.org/10.1021/acs.chemrev.5b00155.

[23] I. Tyrone Ghampson, C. Sepúlveda, R. Garcia, J.L. García Fierro, N. Escalona, W. J. DeSisto, Comparison of alumina- and SBA-15-supported molybdenum nitride catalysts for hydrodeoxygenation of guaiacol, Appl. Catal. A Gen. 435–436 (2012) 51–60, https://doi.org/10.1016/j.apcata.2012.05.039.